A model-based method for damage detection with guided waves

Pouria Aryan[1], Andrei Kotousov[1], CT Ng[2] and B S Cazzolato[1]

[1] School of Mechanical Engineering, University of Adelaide, Adelaide, Australia
[2] School of Civil, Environmental & Mining Engineering, University of Adelaide, Adelaide, Australia

E-mail: andrei.kotousov@adelaide.edu.au

Abstract

Defect detection techniques, which utilise guided waves, have received significant attention over the past twenty years. Many of these techniques implement the baseline signal subtraction approach for damage diagnosis. In this approach, the baseline signal previously recorded for a defect-free structure is compared with/or subtracted from the actual signal recorded during routine inspections. A significant deviation between these two signals (or residual signal/time-trace) can be treated as an indication of the presence of critical damage. However, the accuracy of this common approach can be compromised by various uncontrolled factors, which include ambient temperature variations, unavoidable inconsistences in the PZTs installation procedure and degradation of mechanical properties with time. This paper presents a new method for reconstruction of the baseline signal, which can compensate for the above influences and improve the accurateness of damage diagnosis. The method utilises 3D laser vibrometry measurements in conjunction with high-fidelity FE simulations. This paper also describes an application of this method to the reconstruction of the baseline signal and detection of damage in beam and plate structures.

KEY WORDS: damage detection, guided waves, SHM, transient FE analysis, 3D laser vibrometry, baseline signal.

1. Introduction

During the past two decades, on-line damage detection techniques have been a subject of intensive research and development in many industries and applications. The potential benefits of such techniques are significant and include a step improvement in reliability and safety, along with a substantial reduction in the associated maintenance costs [1]. The on-line damage detection techniques are often based on the generation and sensing of guided waves to detect various types of structural damage, such as cracks [2-9], corrosion spots [10-13], delamination, debonding or matrix damage in composites [14-22].

Guided waves have several special properties which make them very attractive for on-line applications [17, 23, 24]. These include:

(i) An ability to propagate over large distances without significant energy decay and, therefore, can be used for inspection of large areas with a single or small number of actuators/sensors;

(ii) High sensitivity to the presence of various types of structural damage;

(iii) Simplicity, energy and weight efficiency of the hardware, resulting in easy integration of damage detection systems based on guided waves into on-line structural health monitoring systems.

The baseline subtraction approach is often utilised in the guided wave based damage detection techniques to process the recorded signal responses during routine inspections and identify the presence of structural damage [25-28]. In accordance with this approach, the previously recorded signal for a defect-free structure or structural component (the baseline signal) is subtracted from the actual signal obtained during inspections. A significant deviation between these two signals (the critical or threshold level of this deviation depends on the particular application) is treated as an indication of the presence of critical damage. A schematic illustration of the baseline signal subtraction approach for damage detection is shown in Figure 1.

The baseline (signal) subtraction approach can easily be adopted by on-line health monitoring systems due to the above listed properties of guided waves, which normally do not interfere

with operational loads. Another significant advantage of the baseline signal subtraction method is its ability to detect damage in structural components with complex geometry [14].

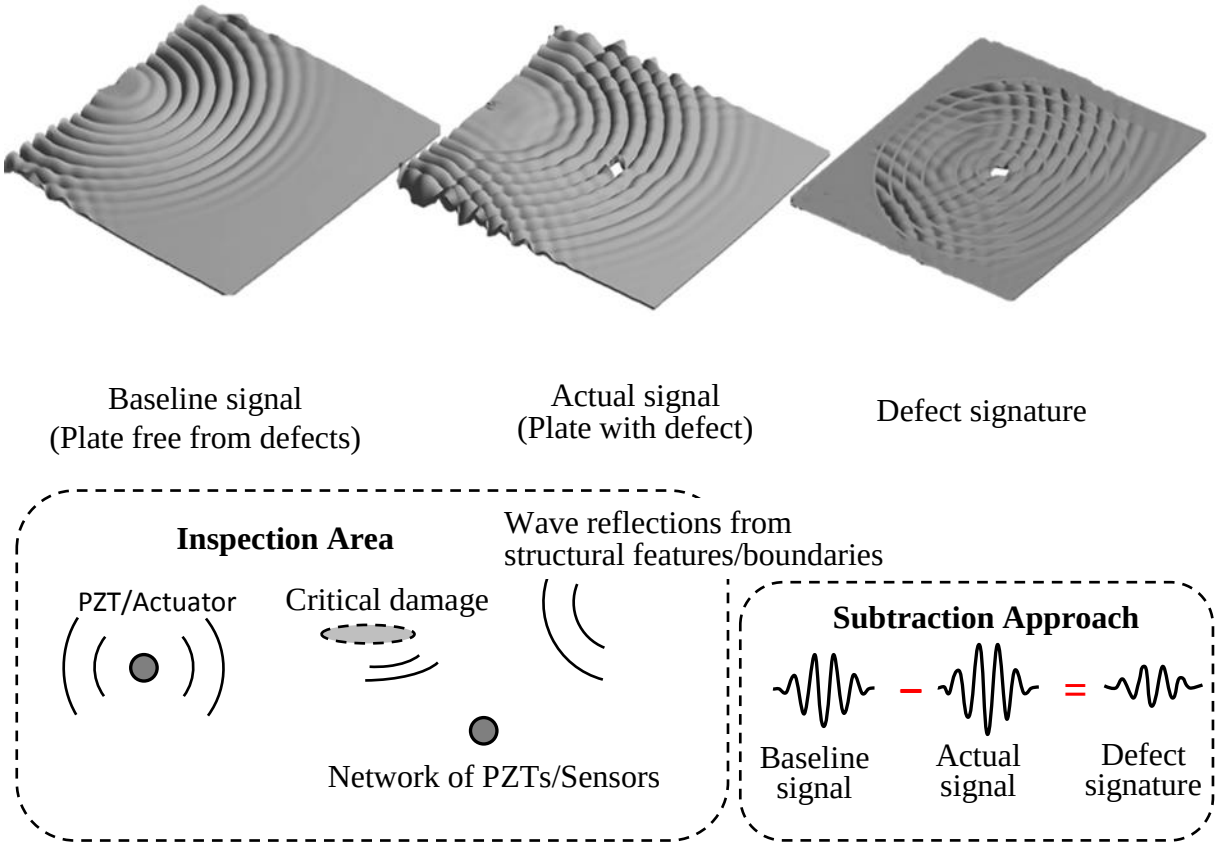

Figure 1: Illustration of the baseline signal subtraction approach for damage detection using guided waves

As it alluded to in the literature, application of this approach in practice, however, can face many obstacles. The accuracy of damage detection can be significantly compromised by a number of uncontrolled factors [14]. In metallic structures, which are the focus of the current paper, these factors include:

(i) Ambient temperature variations, which can affect the response of PZT;

(ii) Variations in PZT adhesive bond thickness and its properties, which can result in large differences in the baseline signals for identical structural components;

(iii) Time in service and severity of loading, which can change the mechanical properties of the structure, adhesive bond and PZT or in some cases even the geometry of the structural component, e.g. due to local buckling.

For example, the effect of the variations in the adhesive thickness on the PZT-induced wave excitation signal was comprehensively investigated in Ha and Chang [29]. In particular, it was demonstrated that small variations in the thickness as small as from 10 μm to 40 μm can significantly influence the generated signal. This means that identical free-from-defect structures with the same material properties could have completely different baseline signal responses due to slight and uncontrollable differences in the bond layer. The same conclusion was derived in a number of past studies focusing on different aspects or inconsistences of PZT installation procedures, such as variations in the mechanical properties of the adhesive sourced from different batches [29-32].

The influence of temperature variations on damage detection with PZTs is well-known and has been extensively documented in the literature [33-37]. Even relatively small temperature variations, say $\pm 10\ ^0$C, can significantly modify the burst signal generated by the PZT due to the changes in the mechanical properties of the adhesive. In addition, for polymer materials and composites, which will be a focus of a separate study, these variations can strongly affect the guided wave propagation and even mask damage [35, 38].

Over the past two decades, a significant effort by many researchers has been devoted to the development of various compensation techniques, which could improve the reliability of the defect detection with guided waves. Several such techniques were reported in the literature, e.g. [34, 38, 39] to name a few. For example, one particular compensation technique [39] combines an adaptive filter and optimisation of the baseline signal to minimise the influence of temperature variations on damage detection.

The present paper proposes a new practical method, which is able to avoid the influence of many uncontrolled factors affecting the baseline signal for free-from-defect structure. Instead of focusing on signal processing techniques [24, 34, 38, 39], it reconstructs the baseline signal corresponding to the current conditions of the structural component and PZTs. This method utilises 3D scanning laser vibrometry (SLV) and transient high-fidelity FE simulations of guided wave propagation.

The conceptual idea of this method is based on a physical recording of the actual 3D velocity/displacement fields around the PZT (scanning area) and prescribing these fields to the corresponding finite element model representing the free-from-defect structure. The scanning

area encapsulates the PZT avoiding the necessity to model the PZT response, which is extremely complex and can be affected by many factors as discussed above. The material properties data, which is needed for the numerical simulations, is extracted from the analysis of the wave propagation in the scanning area of the actual specimen. Therefore, this method can compensate for the possible variations in the material properties of the structure and adhesive bond between the PZT and the structure. The paper demonstrates the feasibility of the accurate reconstruction of the baseline signal with the proposed method. It also describes a practical application of the developed method to damage detection in an isotropic beam structure. In addition, the method can be easily extended for complex structural components or anisotropic materials. However, this will be a subject of future work.

It is recognised that the use of SLV or other 3D measurement systems, as well as high-fidelity transient FE simulations, can significantly increase the cost of the non-destructive defect inspections. However, with the advance of computational power, numerical packages and laser technologies, this cost will eventually decrease exponentially over time. Moreover, this method can be useful for defect inspections of hard-to-reach locations, or for the generation of periodical updates of baseline signals, specifically, in the case of varying loading and temperature conditions.

This paper is organized as follows. The next section introduces the concept of the proposed new method for reconstruction of the baseline signal. Section 3 presents outcomes of transient FE simulations with the overall purpose of demonstrating that the baseline signal can be accurately reconstructed if the area with the prescribed boundary conditions is sufficiently large and the mesh density is appropriately applied. Section 4 provides details of an experimental study conducted to demonstrate the practical reconstruction of the baseline signal for a simple isotropic beam as well as detection of damage with the new method.

2. The Method

The concept of the proposed method can be explained with a help of two spaces; the physical space and modelling space as shown in Figure 2. The physical space represents the actual plate or shell component equipped with an actuator (PZT) generating a burst signal of certain wavelength (frequency). The measurement system incorporates the 3D laser vibrometer (or any other equipment), which is capable of accurately measuring the surface displacements (on the both sides of the component) due to PZT excitation. The surface displacement over the scanning area, which encapsulates PZT, and at a remote location, P, are recorded and utilised in the modelling space for the reconstruction of the baseline signal and defect signature analysis, respectively.

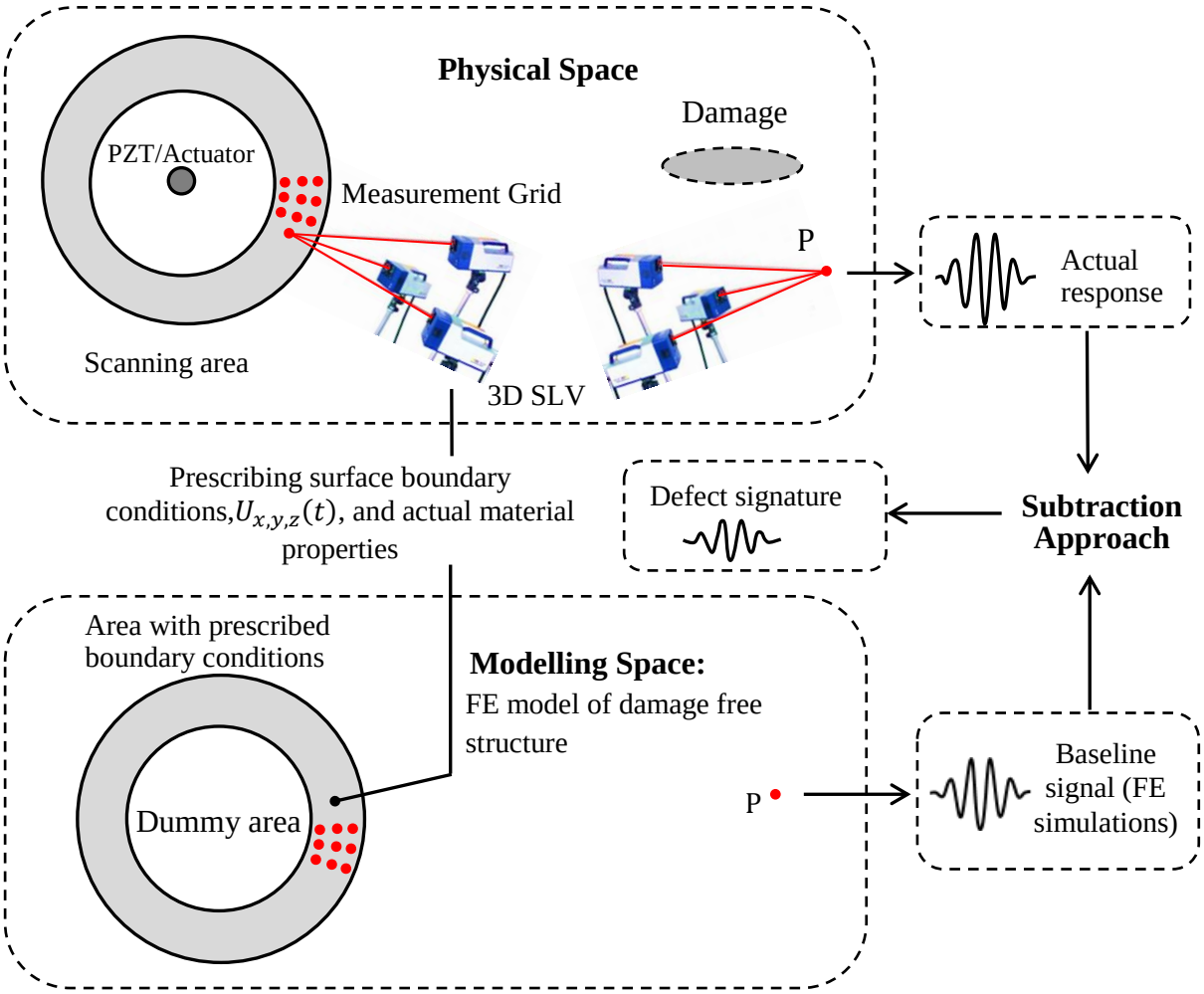

Figure 2: Concept of the method illustrating the physical and modelling spaces.

The modelling (virtual) space represents an accurate FE model of the free-from-defect structural component, with the exception of the dummy region, see Figure 2. The corresponding boundary conditions are applied to the points where the physical measurements were taken in the physical space. It will be demonstrated later in this paper (Section 3) that the wave propagation in this dummy region does not affect the wave dynamics outside the area with the prescribed boundary conditions if the length of this area is larger than the half of the wavelength of the generated signal, so the dummy region, which encircles PZT, can be simply ignored. It will be also confirmed via extensive FE simulations and experimental studies that an accurate baseline signal at a remote location, P, can be obtained (or reconstructed) with the proposed method. Further, the reconstructed baseline signal and the actual responses at the same remote location(s) can be analysed, using, for example, the baseline signal subtraction or any other defect signature evaluation approach.

3. Numerical Implementation of the Method

3.1. Details of Numerical Simulations

This section presents selected outcomes of preliminary numerical simulations of the sensitivity of the reconstructed baseline signal to the size (length, L) of the scanning area. The purpose of these simulations is to help to identify the approximate size of the scanning area and the mesh density, which are necessary for an accurate reconstruction of the baseline signal, as well as to demonstrate the feasibility of the new method for a simple case. With this purpose, two FE models were developed; one represents the physical space (Model 1) and another the modelling space (Model 2), as illustrated in Figure 4. The differences between the models are: (1) Model 2 ignores the area encapsulated by the scanning area (shown by dotted lines in Figure 3), and (2) the boundary conditions (displacements) in Model 2 are extracted from the scanning area of Model 1. These arrangements virtually simulate the proposed method for the reconstruction of the baseline signal in the simplest case of a beam component. The symmetry boundary conditions are applied to the edges of the beam, so the wave propagation is essentially 2D process, with zero displacements in the lateral direction, $U_y = 0$. Also, for convenience, the simulations were limited to linear-elastic, isotropic and homogeneous materials.

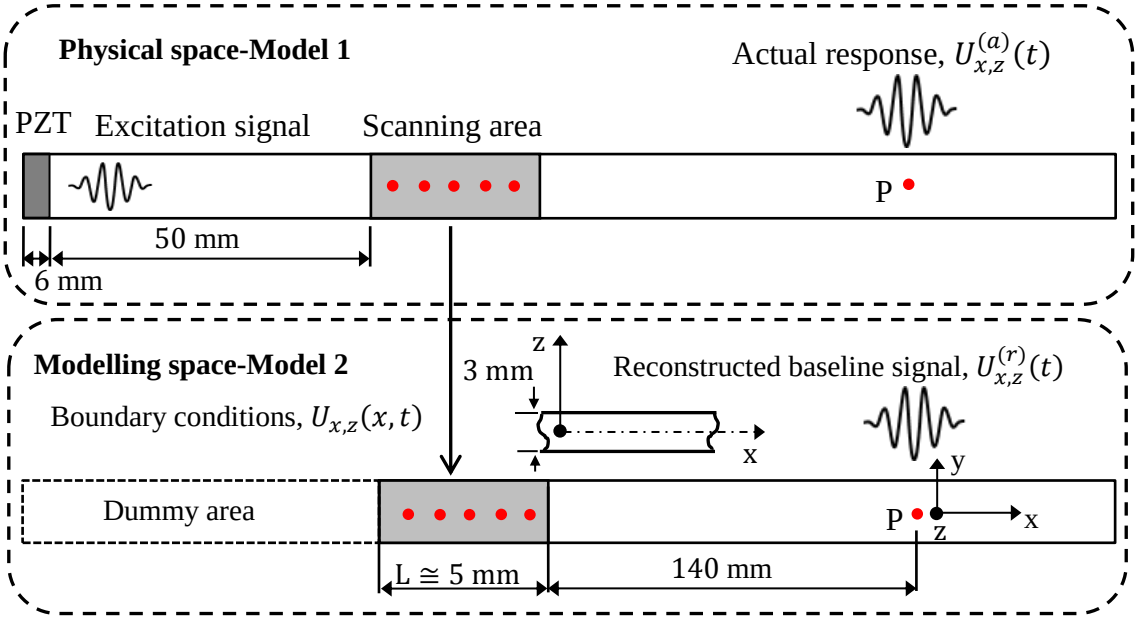

Figure 3: Virtual implementation of the proposed method for a 1D isotropic homogeneous beam and f = 200 kHz excitation frequency.

The scanning area is now reduced to a line with a characteristic length, L. The 2D surface velocity components from Model 1 (the physical space), $U_z(t, x, z = \pm h/2)$ and $U_x(t, x, z = \pm h/2)$, were prescribed as boundary conditions for Model 2 (the modelling space) as described above, and two displacements as computed by two models, $U_{x,z}^{(a)}(t)$ and $U_{x,z}^{(r)}(t)$, can be then compared at a remote location, e.g. point P shown in Figure 4. From this comparison we can evaluate the error associated with the baseline signal reconstruction method. This error provides essential information for the selection of the appropriate threshold signal level, which can be adopted for the identification of the presence of critical damage.

A 2D explicit FE model representing an isotropic homogeneous beam with 0.3 mm × 3 mm cross section was developed using the ANSYS 15.0 software package. The FE model utilised 3D hexahedral type of element with hourglass control. Each node of the hex element had two displacement degrees of freedoms. The pure A0 and S0 mode guided waves were excited by applying the corresponding nodal displacements to the surface nodes representing the PZT transducer area, see Figure 3. The length of this area is 3 mm, and it was located at the left end of the beam. A very fine mesh with the typical element size 0.25 × 0.25 × 0.25 mm^3 was used in the finite element models. This element size corresponds to 0.05λ, (or 20 nodes per wavelength), which exceeds the minimum required number of nodes per wavelength reported in the literature [28, 40].

The transient (guided wave propagation) problem was solved by AutoDyne solver. The standard elastic properties used in the numerical simulations; Young's modulus (E) of 72 GPa and Poisson's ratio (ν) of 0.3, which correspond to aluminium alloys. A five-cycle sinusoidal tone burst modulated by a Hanning window, was used to generate anti-symmetric (A0) and symmetric (S0) modes of the burst signal,

$$U_z(t) = A\left(1 - \cos\frac{2\pi f t}{N}\right)\cos(2\pi f t) \qquad (1)$$

where $U_z(t)$, are the prescribed displacements in the PZT area in z direction to excite S_o and A0, respectively, A is the amplitude of the pulse, $f = \omega/(2\pi)$ is the pulse centre frequency, t is the time and N is number of the generated cycles (which in this case N = 5). The A0-mode of guided wave was generated by applying the same displacements on the both free surfaces of the beam, while the S0-mode was generated when the sign of the applied displacement on the free surfaces of the beam is opposite. These boundary conditions correspond to two PZT patches placed on the top and bottom surfaces of the beam subjected to the same or opposite polarity signal bursts. The time step was automatically controlled by ANSYS/AutoDyne and depended on the smallest element size.

3.2 Selected Numerical Results

Typical results of the numerical simulations are presented in Figure 4. This figure demonstrate the influence of the length ($L = a\lambda$) of the scanning area on the accuracy of the reconstructed baseline signal. Here λ is the wavelength corresponding to the excitation frequency, f, and a is a coefficient representing the ratio of the length of the scanning area to the wavelength.

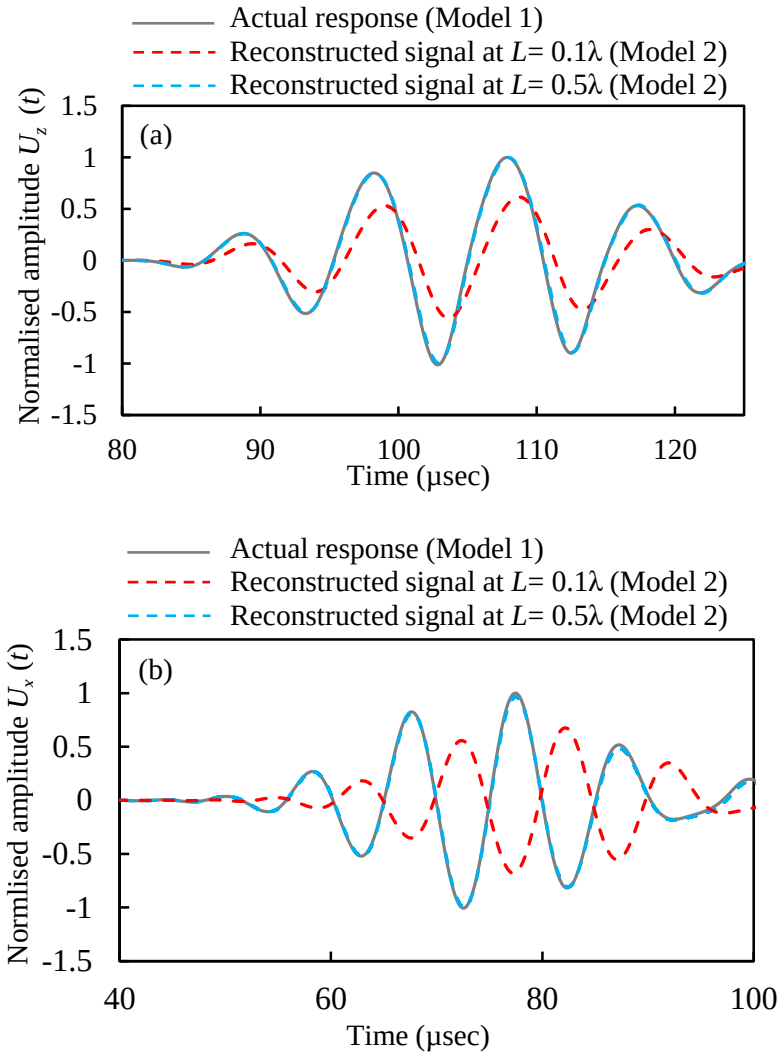

Figure 4: Comparisons of the generated baseline signal (Model 1) with the reconstructed baseline signal (Model 2) at a remote point for f =100 kHz excitation frequency, (a) out-of-plane displacement U_z, (b) in-plane displacement U_x. At L= 0.5λ the difference between the actual response (Model 1) and the reconstructed signal (Mode 2) is negligible.

The main outcome of the numerical simulations (or virtual implementation of the proposed method) is that the baseline signal can be reliably reconstructed when the length of the scanning area L= 0.5λ or $a \geq 0.5$) with the mesh density corresponding to approximately twenty measurements points per wavelength of the excited signal. The accuracy is slightly lower for the in-plane displacements, which are associated with S_o mode (see Figure 4). The discrepancies between the reconstructed, $U_{x,z}^{(r)}(t)$, and the actual signals, $U_{x,z}^{(a)}(t)$, for the S0 mode can also be attributed to the accuracy of the numerical simulations, which can be improved by selecting a higher mesh density and a smaller time step, if required. From our numerical simulations it was

also demonstrated that the similar recommendations for the selection of mesh density and the length of the scanning area apply to plates as well. In the next section the proposed method will be applied to generate the baseline signal and detect damage in a beam and plate structures.

4. Experimental Studies

The purpose of this section is to demonstrate a practical application of the developed method to the reconstruction of the baseline signal, as well as for damage detection. In the beginning the experimental set up will be described, after that the reconstruction procedure of the baseline signal from the actual scanning data obtained from the 3D SLV will be applied, and finally, the baseline substruction approach based on the reconstructed baseline signal will be utilised to detect damage in simple structures.

4.1 Experimental Rig

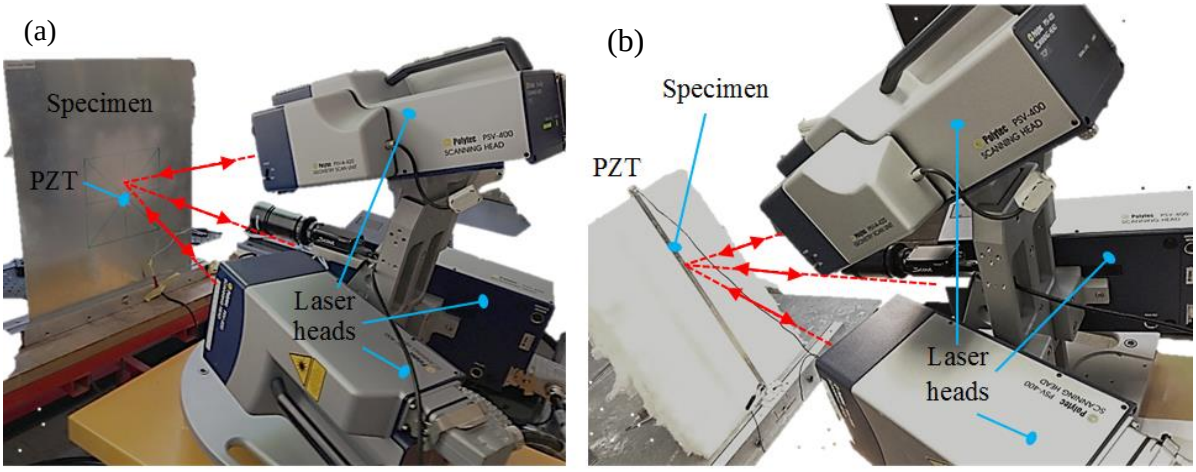

Figure 5: Experimental rig (a) the aluminium plate and (b) the aluminium beam.

The experimental rig is shown in Figure 5. The specimens utilised in the experimental studies represent a 3 mm thick square plate 500mm by 500mm, see Figure 5(a) and a beam of 3 mm× 12 mm cross-section and 300 mm long, see Figure 5(b). Both specimens were cut from the same bulk plate made of aluminium alloy. For wave generation in the plate sample, a disk-shaped PZT of 10 mm in diameter and 3 mm in thickness with a backing mass of the same size made of brass were glued on the surface in the centre of the plate, see Figure 5(a). A rectangular-

shaped PZT of in-plane dimensions 12 mm by 6 mm and 2 mm thick with a backing mass of the same size but 3 mm in thickness, made of brass was glued on the surface of one end of the beam specimen. The backing masses were used to maximise the excitability of the A0 mode guided wave. The experimental equipment included a power amplifier, 3D scanning laser vibrometer and a built–in signal generator. A five-cycle sinusoidal tone burst modulated by a Hanning window, at frequencies between 100 to 300 kHz, was generated using a signal generator and amplified, up to ±50 V, using the power amplifier. This amplified signal was applied to the transducer mounted on the surface of the beam specimen. The transducer transformed the amplified electrical signal to the surface displacements that generate the guided wave. The signal was excited and recorded 200 times for each experimental arrangement, averaged and filtered to remove noise and systematic errors. The interval between consecutive signals was 9 ms, which is sufficient to avoid the interference between the signals and responses. The data recording and signal generation stages were synchronized accurately and controlled by the SLV computer.

The out-of-plane, $V_z(t)$, and in-plane, $V_x(t)$ and $V_y(t)$, velocity fields were measured on both surfaces of the beam by a Polytec PSV-400 SLV. The PSV-400 SLV consists of three separate scanning heads and utilises the Doppler effect for measurement of velocities in three directions. With a simple coordinate transformation, these measured velocities can be resolved in the x, y and z directions. These velocity components were temporally integrated using a built-in SLV computer to obtain the displacement field at the grid point locations.

To simplify the prescription of boundary conditions the measurement grid size was selected to be exactly the same as in the numerical simulations. This selected grid size is approximately 20 points per wavelength of A0 mode as found in Section 3.2. The measured signal was averaged 200 times at each measurement point to improve the signal-to-noise ratio (SNR). Inbuilt band pass filters were adjusted such that the lower and higher cut off frequencies were either ±50 kHz or ±100 kHz of the signal envelope energy of each centre frequency, and were applied to reduce the noise outside of the frequency bandwidth. Finally, a sensitivity of 10 mm/s/V, a sampling frequency of 2.5 MHz and a resolution of 390.6 ns were used for the 3D measurements of the velocity fields.

4.2 Defining material properties

In the case of possible changes (or degradation) of material properties, the actual material properties corresponding to the current conditions of defect inspection can be identified from the wave propagation characteristics. There are several well-known techniques for recovery of material properties, for example, from the measured phase velocity dispersion relation for isotropic homogeneous plates. In accordance with this technique, the experimental data can be curve fitted to the theoretical equation [41];

$$C_{ph}(f) = \left[\frac{\rho}{E}\frac{\rho}{\mu}(1-\nu^2) - \frac{\rho}{E}\frac{12}{h^2}(1-\nu^2)\frac{1}{2\pi f^2}\right] \quad (2)$$

where C_{ph} is the phase velocity, ω is the frequency, ρ is the density of the material, h is the plate thickness, E is Young's modulus, μ is shear modulus and ν is Poisson's ratio.

The phase velocity, which is the ratio of the angular velocity, ω, and wavenumber, k,

$$C_{ph}(f) = \frac{2\pi f}{k(f)} \quad (3)$$

can be determined from the phase spectra of time-dependent signals, measured at points along the radial lines, which starts from the excitation source (PZT) [42]. If $\Delta r = (r_2 - r_1)$ is the distance between such two points, and $\Delta\phi(f)$ is the phase difference as a function of a frequency, f, determined from the Fourier transformed signal, then the wavenumber $k(f)$ and the phase velocity can be calculated as

$$k(f) = -\frac{\Delta\phi}{\Delta r} \quad (4)$$

and

$$C_{ph}(f) = -\frac{2\pi f \Delta r}{\Delta\phi} \quad (5)$$

In order to avoid $\pm 2n\pi$ ambiguity, several measurement points along the radial line can be taken, so the value of n can be identified. The measuring points have to be selected in the way that the approximation of the centrally induced flexural waves by plane waves is reasonably accurate and that the input signal has passed the measurement point before the first reflection arrives.

Once the phase velocity, $C_{ph}(f)$, is determined using least square optimisation and E/ρ as the parameter to be fit in Eq. (2), the actual value of this ratio can be identified, provided all other parameters, such as thickness and Poisson's ratio are known. An application of this technique to the identification of the ratio E/ρ is shown in Figure 6. Here, the phase velocity was

measured for the 3 mm thickness aluminium plate subjected to A0 mode excitation. Assuming Poisson's ratio, ν = 0.3, (in general, it does not significantly affect the optimisation result) $E/\rho = 28.5$ MN/kg was obtained and used in the numerical reconstruction of base-line signals for beam and plate geometries.

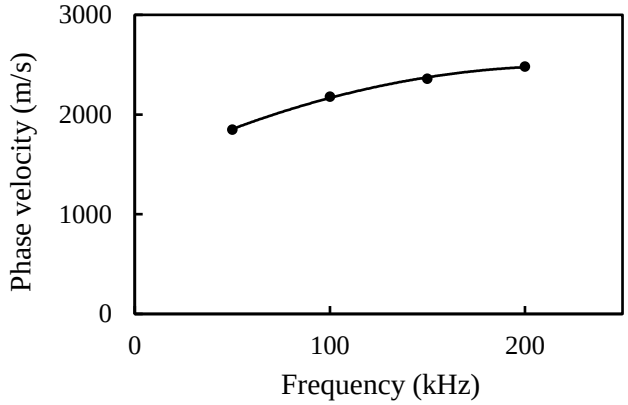

Figure 6: Phase velocity measurements and the fitted curve for the 3mm thickness aluminium plate. The dots represent the measured phase velocity at discrete frequencies.

According to Glushkov *et al.* (2015) [43] the phase velocity between beam and plate are not identical but the difference is very small, especially at lower frequency ranges (below 200kHz). Hence, for the beam it is still possible to use the material properties obtained from the phase velocity curve of the plate.

If several parameters are unknown then a multi-parametric optimisation can be conducted in order to recover the actual material properties of the structure. It is clear that the size and the shape of the scanning area have to be adequate for the determination of the phase velocity and recovery of the material properties. These issues were previously investigated in a number of articles for both isotropic and anisotropic materials [44-48] and will not be repeated in this paper.

4.3 Example of Reconstruction of Baseline Signal

Initially, the measurements were conducted for only one single row of the sample points on the top and bottom of the beam located in the middle of the scanning area as shown in Figure 3.

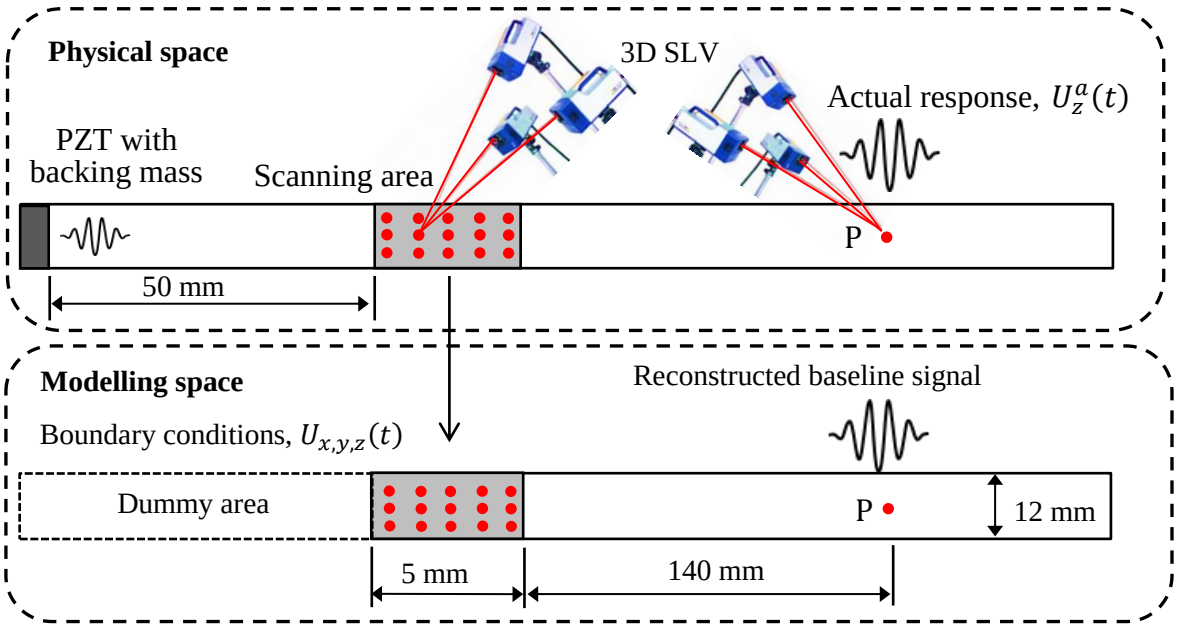

Figure 7: Experimental implementation of the proposed method for a 1D isotropic beam.

The obtained experimental results were compared with the results from the numerical simulations using the proposed method as described in the previous section. Large discrepancies can be observed, see Figure 8(a), between the actual and reproduced baseline signals. These discrepancies between the modelling and experimental results were attributed to the effect of wave reflection from the beam edges, indicating that the wave propagation along the beam is essentially a 3D process. Therefore, to increase the accuracy of the method we considered several rows of measurement points across the width of the specimen. For example, Figure 8(b) shows the comparison of the actual $U_z^{(a)}(t,P)$ displacement function recorded by SLV with the displacement function, $U_z^{(r)}(t,P)$, obtained from the corresponding FE model in the case of three rows of measurement points across the beam width, exactly as shown in Figure 7. As it can be seen from Figure 8(b) the difference between the reconstructed and actual baseline signal is now quite small, and can be further decreased with the application of higher mesh density, reduction of the time step and improvement of the accuracy the measurements with SLV.

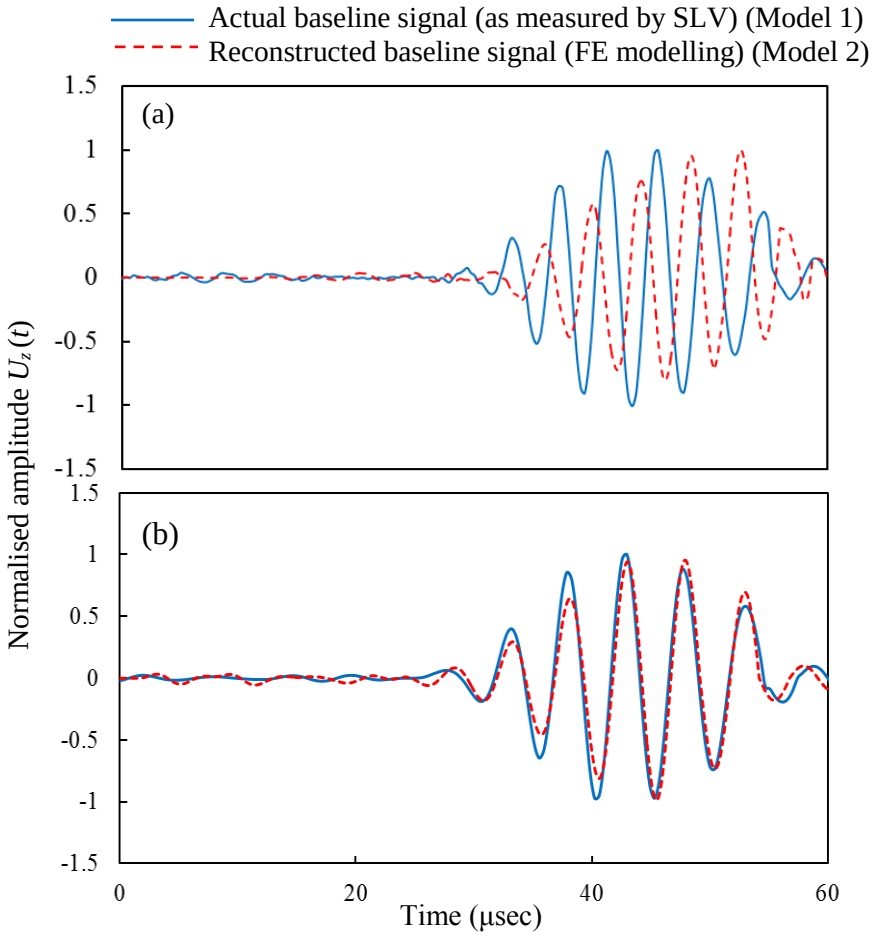

Figure 8: Comparison between results of the physical and modelling spaces (Model 1 and Model 2) for out-of-plane displacement U_z for f =200 kHz for (a) one row and (b) three rows of measurement points.

The algebraic subtraction of the two signals in Figure 8(b) is shown in Figure 9. It is clear that for practical applications of the proposed method in damage detection techniques, the amplitude of this signal, which essentially represents the error associated with the reconstruction method, has to be much smaller than the threshold signal adopted for the particular structure and type of the damage.

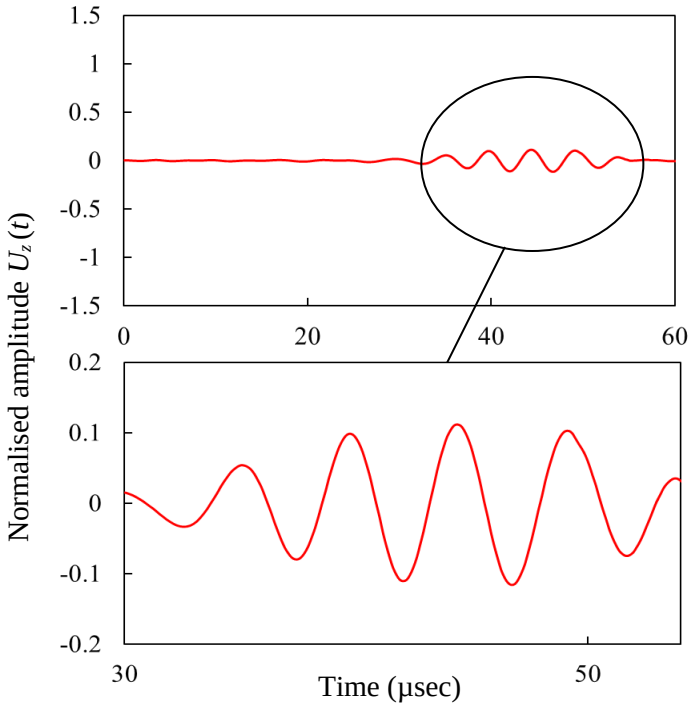

Figure 9: Subtracted signal between measured and reconstructed baseline signals of the out-of-plane displacement U_z demonstrating the error associated with the method.

4.4 Detection of Damage

This section details the application of the developed method for the detection of damage in a simple beam structure. A half-cylindrical volume was milled at the free surface of the beam at a distance of 100 mm from the PZT (excitation source). The cross sectional dimensions of the milled volume are 2×1×12 mm^3 as illustrated in Figure 10.

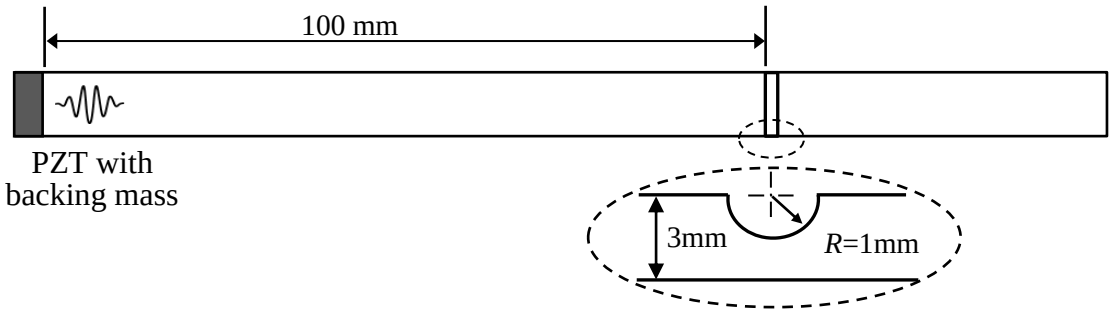

Figure 10: Schematic of the specimen with the introduced damage. All other dimensions are as shown in Figure 7.

Figure 11 shows the reconstructed baseline signal for defect-free structure, based on the proposed method, as well as the signal recorded by SLV for the damaged beam shown in Figure 10. A significant difference between these two signal responses can be easily identified. Figure 12 shows the comparison of (1) the subtracted actual signal of damaged structure with the reconstructed baseline signal and (2) the error between the reconstructed baseline signal and the actual baseline signal, which was also presented previously in Figure 9. It can be noted from Figure 12 that the error associated with the reconstruction method is significantly smaller than the damage signature. This provides the confidence that the difference between the reconstructed baselines signal and the actual signals are not due to numerical errors but are because of the presence of the damage.

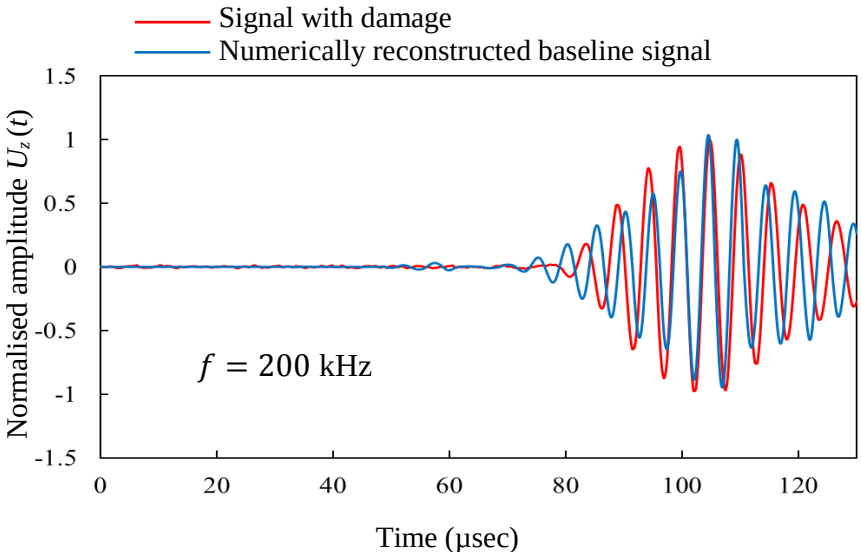

Figure 11: Reconstructed baseline signal (with the proposed method) and the actual signal for beam with a damage (Figure 10).

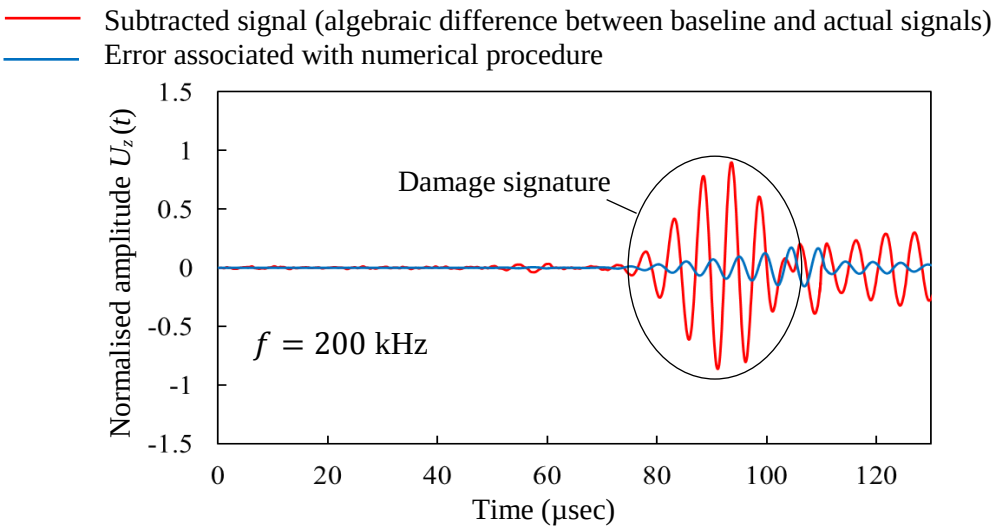

Figure 12: Comparison of subtracted signal (out-of-plane displacements U_z) of damaged structure with reconstructed baseline and error associated with the proposed method (difference between actual and reconstructed baseline signals).

The next example demonstrates the application of the proposed method for the detection of damage in the case of plate geometry. A narrow slit of 10 mm length and 2 mm width and 1.5 mm depth was milled at a distance of 70 mm from PZT in the aluminium plate of 3 mm thickness. The same method for the numerical reconstruction of the baseline signal and the same parameters of FE model were implemented for the plate (as illustrated in Figure 2). The reconstructed baseline signal was compared with the actual signal affected by the damage and recorded with SLV. Figure 13 shows the subtracted signal, which represents the algebraic difference between the numerically reconstructed baseline and actual signals. Similar to the previous case with the beam geometry (Figure 10), the error associated with the reconstruction method is much smaller than the damage signature. Therefore, the considered type of damage in plates can also be reliably identified with the proposed method.

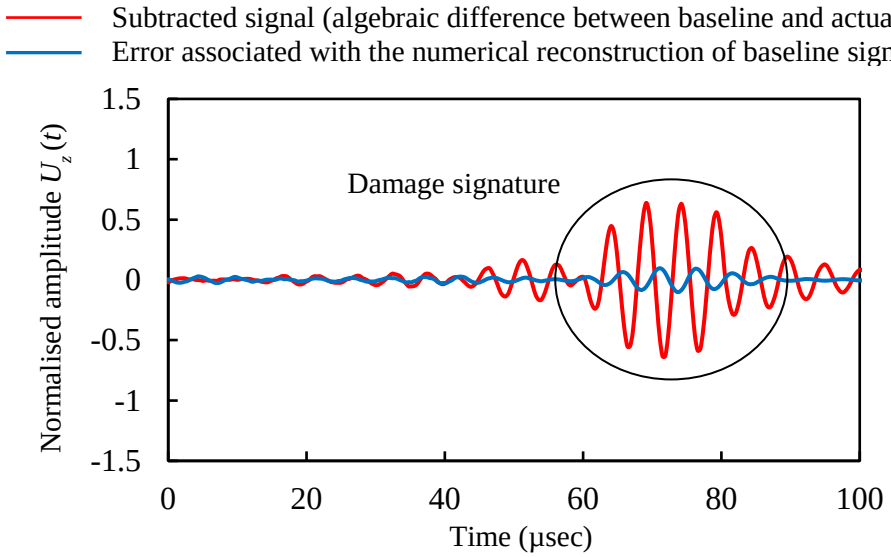

Figure 13: Reconstructed baseline signal (with the proposed method) and the actual signal for a damaged plate for the out-of-plane displacement U_z and for f =200 kHz excitation frequency.

In a general case, the accuracy of the reconstructed signal, or, essentially the complexity of the FE model, density of the measurement points and the accuracy of the measurements, has to be appropriately selected based on the magnitude of the signal threshold accepted as the indication of damage in accordance with the baseline signal substruction approach. This magnitude depends on the particular application and type of damage as discussed above. Therefore, the selection of the parameters, such as time step in numerical simulation, density of the measurement points, requires extensive preliminary numerical simulations as well as experimental studies in order to verify that the accuracy of the reconstructed signal is sufficient to detect the critical damage. However, once the accuracy is verified then the method can be routinely applied to the similar structures working under variable ambient temperature or loading conditions. It is clear, that the damage diagnosis for more complicated structures will require a more extensive computational effort, and currently, the method can be applicable to rather simple geometries. However, this should not be a critical problem in the future taking into account a very rapid development of numerical techniques and continuing increase in computer power.

5. Conclusions

A new method to reconstruct or update baseline signals for damage detection with guided waves was presented in this paper. The proposed method utilises 3D scanning laser vibrometry measurements in conjunction with explicit high-fidelity FE simulations of guided wave propagation in a free-from-defect structure. This method can help to overcome the current difficulties associated with the necessity to compensate for the uncontrolled factors affecting the baseline signal, such as temperature variations, various uncertainties in PZT installation procedure and material degradation. The current paper focuses on one-dimensional waveguides, i.e. the guided waves in beam and plate structures. The conducted numerical and experimental studies have demonstrated the concept and practicality of the proposed method. In particular, it was demonstrated that the baseline signal can be reconstructed based on the measurements of the displacement field near the actuator and prescribing these fields to the corresponding FE model, which represent the free-from-defect structure. It is important that the region encapsulated by the scanning area can be disregarded in the FE simulations if the length of the scanning area (see Figure 2) is sufficiently large, say larger than the half of the wavelength of the excitation signal. Thus, this avoids the need to model the PZT response, which can be affected by many factors. Another important aspect of the method is that the accuracy of the generation of the reconstructed baseline signal can be controlled by selecting the appropriate mesh density, time step and accuracy of the measurements. The method is capable of taking into account the changes in material properties of the structural element by analysing the guided wave propagation for different frequencies and extracting the actual material properties from the generated experimentally dispersion curves.

The paper also described a practical implementation of the new method to simple isotropic beams and plates. The experimental studies were underpinned by numerical simulations, which demonstrated the feasibility of this method and guided the selection of the governing parameters of the method. It is recognised that the utilisation of 3D measurement system and transient FE simulations can significantly increase the cost of the damage detection. Moreover, wave propagation in complex structures (e.g. riveted panels or composite sandwich panels) is still represent a significant challenge for numerical modelling However, it is believed, that with the advance of computer and laser technologies the cost-efficiency can be significantly improved, and, in the future, the proposed method can be utilised to detect damage in many practical applications and more complex structures than considered in the current study.

The future work will be primary directed to composite components, where guided wave based defect detection techniques are considered to be a very promising for the development of on-line health monitoring systems. However, in the case of composite structures, the required size of the scanning area may be significantly larger as a result of a much more complicated wave structure generated by actuator (PZT) and the necessity to identify more material constants for accurate reconstruction of the baseline signal.

Acknowledgement

This work was supported by the Australian Research Council (ARC) under Grant Number DE130100261.

References

1. Wildy SJ, Kotousov A, Codrington J. A new passive defect detection technique based on the principle of strain compatibility. *Smart Materials and Structures* 2008; **17**(4): 045004-12.

2. Fromme P, Sayir MB. Detection of cracks at rivet holes using guided waves. *Ultrasonics* 2002; **40**(1): 199-203.

3. Ge L, Wang X, Jin C. Numerical modeling of PZT-induced Lamb wave-based crack detection in plate-like structures. *Wave Motion* 2014; **51**(6): 867-885.

4. Lu Y, Ye L, Su Z,Yang C. Quantitative assessment of through-thickness crack size based on Lamb wave scattering in aluminium plates. *NDT & E International* 2008; **41**(1): 59-68.

5. Tian Z, Leckey C, Rogge M, Yu L. Crack detection with Lamb wave wavenumber analysis. *SPIE Smart Structures and Materials+ Nondestructive Evaluation and Health Monitoring* 2013; **8695**: 86952Z-13.

6. Zhou L, He Z, Sun H. Lamb wave mode conversion-based crack detection for plate-like structures without baseline information. *Journal of Vibroengineering* 2013; **15**(2): 647-57.

7. Leong W H, Staszewski W J, Lee BC, Scarpa F. Structural health monitoring using scanning laser vibrometry: III. Lamb waves for fatigue crack detection. *Smart Materials and Structures* 2005; **14**: 1387-95.

8. Yao Y, Tung S-T E, Glisic B. Crack detection and characterization techniques—An overview. *Structural Control and Health Monitoring* 2014; **21**(12): 1387-1413.

9. Staszewski W J, Lee BC, Traynor R, Fatigue crack detection in metallic structures with Lamb waves and 3D laser vibrometry. *Measurement Science and Technology* 2007; **18**(3): 727-739.

10. Pei J, Yousuf MI, Degertekin FL, Honein BV, Khuri-Yakub BT. Lamb wave tomography and its application in pipe erosion/corrosion monitoring. *Research in Nondestructive Evaluation* 1996; **8**(4): 189-197.

11. Jenot F, Ouaftouh M, Duquennoy M, Ourak M. Corrosion thickness gauging in plates using Lamb wave group velocity measurements. *Measurement Science and Technology* 2001; **12**(8): 1287-1293.

12. Sharma S, Mukherjee A. Ultrasonic guided waves for monitoring corrosion in submerged plates. *Structural Control and Health Monitoring* 2015; **22**(1): 19-35.

13. Ng C T. Bayesian model updating approach for experimental identification of damage in beams using guided waves. *Structural Health Monitoring* 2014; 14759217-14532990.

14. Yeum C M, Sohn H, Lim H, Jin I, Jeong B. Reference-free delamination detection using Lamb waves. *Structural Control and Health Monitoring* 2013; **21**(5): 675-684.

15. Sohn H, Swenson E D, Olson S E, DeSimio M P, Dutta D. Delamination detection in composite structures using laser vibrometer measurement of Lamb waves. *Health Monitoring of Structural and Biological Systems* 2012; **7650**: 76500P1-10.

16. Ng CT, Veidt M, Rose LRF, Wang CH. Analytical and finite element prediction of Lamb wave scattering at delaminations in quasi-isotropic composite laminates. *Journal of Sound and Vibration* 2012; **331**(22): 4870-4883.

17. Su Z, Ye L, Lu Y. Guided Lamb waves for identification of damage in composite structures: A review. *Journal of Sound and Vibration* 2006; **295**(3–5): 753-780.

18. Ng CT, Veidt M. Scattering of the fundamental anti-symmetric Lamb wave at delaminations in composite laminates. *The Journal of the Acoustical Society of America* 2011; **129**: 1288-1296.

19. Sohn H, Park G, Wait J R, Limback N P, Farrar C R, Wavelet-based active sensing for delamination detection in composite structures. *Smart Materials and Structures* 2004; **13**: 153-160.

20. JP M, Balasubramaniam K, Lamb-wave-based structural health monitoring technique for inaccessible regions in complex composite structures. *Structural Control and Health Monitoring* 2014; **21**(5): 817-832.

21. Chia C C, Hyo-Mi J, Jung-Ryul L, Gyuhae P, Composite aircraft debonding visualization by laser ultrasonic scanning excitation and integrated piezoelectric sensing. *Structural Control and Health Monitoring* 2012; **19**(7): 605-620.

22. Staszewski W J, Mahzan S, Traynor R, Health monitoring of aerospace composite structures–Active and passive approach. *Composites Science and Technology* 2009; **69**(11): 1678-1685.

23. Pavlopoulou S, Staszewski W J, Soutis C, Evaluation of instantaneous characteristics of guided ultrasonic waves for structural quality and health monitoring. *Structural Control and Health Monitoring* 2013; **20**(6): 937-955.

24. Dao P B, Staszewski W J, Lamb wave based structural damage detection using cointegration and fractal signal processing. *Mechanical Systems and Signal Processing* 2014. **49**(1–2): 285-301.

25. Konstantinidis G, Drinkwater B, Wilcox P. The temperature stability of guided wave structural health monitoring systems. *Smart Materials and Structures* 2006; **15**(4): 967-976.

26. Clarke T, Cawley P, Wilcox P D, Croxford A J. Evaluation of the damage detection capability of a sparse-array guided-wave SHM system applied to a complex structure under varying thermal conditions. *Ultrasonics, Ferroelectrics, and Frequency Control, IEEE Transactions on* 2009; **56**(12): 2666-2678.

27. McKeon P, Yaacoubi S, Declercq NF, Ramadan S, Yaacoubi WK. Baseline subtraction technique in the frequency–wavenumber domain for high sensitivity damage detection. *Ultrasonics* 2014; **54**(2): 592-603.

28. Ng C T, Veidt M. A Lamb-wave-based technique for damage detection in composite laminates. *Smart Materials and Structures* 2009; **18**(7): 074006-074018.

29. Ha S, Chang F-K. Adhesive interface layer effects in PZT-induced Lamb wave propagation. *Smart Materials and Structures* 2010; **19**(2): 025006-025015.

30. Bhalla S, Soh CK. Electromechanical impedance modeling for adhesively bonded piezo-transducers. *Journal of intelligent material systems and structures* 2004; **15**(12): 955-972.

31. Rabinovitch O, Vinson JR. Adhesive layer effects in surface-mounted piezoelectric actuators. *Journal of intelligent material systems and structures* 2002; **13**(11): 689-704.

32. Islam M, Huang H. Understanding the effects of adhesive layer on the electromechanical impedance (EMI) of bonded piezoelectric wafer transducer. *Smart Materials and Structures* 2014; **23**(12): 125037-125051.

33. Putkis O, Dalton RP, Croxford AJ. The influence of temperature variations on ultrasonic guided waves in anisotropic CFRP plates. *Ultrasonics* 2015; **60**(0): 109-116.

34. Lu Y, Michaels JE. A methodology for structural health monitoring with diffuse ultrasonic waves in the presence of temperature variations. *Ultrasonics* 2005; **43**(9): 717-731.

35. Clarke T, Simonetti F, Cawley P, Guided wave health monitoring of complex structures by sparse array systems: Influence of temperature changes on performance. *Journal of Sound and Vibration* 2010; **329**(12): 2306-2322.

36. Ha S, Lonkar K, Mittal A, Chang FK. Adhesive layer effects on PZT-induced Lamb waves at elevated temperatures. *Structural Health Monitoring* 2010; **9**(3): 247-256.

37. Di Scalea FL, Salamone S. Temperature effects in ultrasonic Lamb wave structural health monitoring systems. *The Journal of the Acoustical Society of America* 2008; **124**(1): 161-174.

38. Croxford AJ, Moll J, Wilcox PD, Michaels JE. Efficient temperature compensation strategies for guided wave structural health monitoring. *Ultrasonics* 2010; **50**(4–5): 517-528.

39. Wang Y, Gao L, Yuan S, Qiu L, Qing X. An adaptive filter–based temperature compensation technique for structural health monitoring. *Journal of Intelligent Material Systems and Structures* 2014; **25**(17): 2187-2198.

40. Lowe M J S, Cawley P, Kao JY, Diligent O. The low frequency reflection characteristics of the fundamental antisymmetric Lamb wave a from a rectangular notch in a plate. *The Journal of the Acoustical Society of America* 2002; **112**(6): 2612-2622.

41. Rose J L. Ultrasonic Waves in Solid Media. *New york: Cambridge University Press* 2014.

42. Veidt M, Sayir M, Experimental evaluation of global composite laminate stiffnesses by structural wave propagation. *Journal of composite materials* 1990; **24**(7): 688-706.

43. Glushkov E, Glushkova N, Eremin A, Giurgiutiu V, Low-cost simulation of guided wave propagation in notched plate-like structures. *Journal of Sound and Vibration* 2015; **352**: 80-91.

44. Ong WH, Rosalie C, Rajic N, Chiu W K. Determination of Elastic Properties in a Plate by Lamb Wave Analysis and Particle Swarm Optimisation. *Procedia Engineering* 2014; **75**: 39-44.

45. Hayashi Y, Shingo O, Hideo C, Takemoto M. Non-contact estimation of thickness and elastic properties of metallic foils by laser-generated Lamb waves. *NDT & E International* 1999; **32**(1): 21-27.

46. Eremin A A, Glushkov E V, Glushkov N V. Lammering R. Evaluation of effective elastic properties of layered composite fiber-reinforced plastic plates by piezoelectrically induced guided waves and laser Doppler vibrometry. *Composite Structures* 2015; **125**: 449-458.

47. Ambrozinski L, Packo P, Pieczonka L, Stepinski T, Uhl T, Staszewski W J. Identification of material properties–efficient modelling approach based on guided wave propagation and spatial multiple signal classification. *Structural Control and Health Monitoring* 2015; **22**(7): 969-983.

48. Spencer A B, Worden K, Staszewski W J, Rongong J A, Sims N D. An Optimisation Scheme Based on the Local Interaction Simulation Approach and Lamb Waves for Elastic Property Estimation in Multi-Layered Composites. *Shock and Vibration* 2012; **19**(5): 1027-1040.